Optical spectroscopy and ultrafast pump-probe study of a quasi-one-dimensional charge density wave in CuTe

R. S. Li,[1] L. Yue,[1] Q. Wu,[1] S. X. Xu,[1] Q. M. Liu,[1] Z. X. Wang,[1] T. C. Hu,[1] X. Y. Zhou,[1] L. Y. Shi,[1] S. J. Zhang,[1] D. Wu,[2] T. Dong,[1] and N. L. Wang[1,3,*]

[1]*International Center for Quantum Materials, School of Physics, Peking University, Beijing 100871, China*

[2]*Songshan Lake Materials Laboratory, Dongguan, Guangdong 523808, China*

[3]*Beijing Academy of Quantum Information Sciences, Beijing 100913, China*

(Received 5 October 2021; revised 24 January 2022; accepted 15 February 2022; published 1 March 2022)

CuTe is a two-dimensional (2D) layered material; yet it forms a quasi-one-dimensional (quasi-1D) charge-density-wave (CDW) along the *a* axis in the *ab* plane at high transition temperature $T_{\mathrm{CDW}} = 335$ K. However, the anisotropic properties of CuTe remain to be explored. Here, we performed combined transport, polarized infrared reflectivity, and ultrafast pump-probe spectroscopy studies to investigate the underlying CDW physics of CuTe. Polarized optical measurements clearly revealed that an energy gap gradually forms along the *a* axis upon cooling, while optical evidence of a gap signature is absent along the *b* axis, suggesting pronounced electronic anisotropy in this quasi-2D material. Time-resolved optical reflectivity measurements revealed that the amplitude and relaxation time of photoexcited quasiparticles change dramatically across the CDW phase transition. Performing fast Fourier transformation of the oscillation signals arising from collective excitations, we identify the 1.65-THz mode as the CDW amplitude mode, whose energy softens gradually at elevated temperatures. Consequently, we provide further evidence for the formation of completely anisotropic CDW order in CuTe, which is quite rare in quasi-2D materials.

DOI: 10.1103/PhysRevB.105.115102

I. INTRODUCTION

Charge density waves (CDWs) have been of great interest in condensed matter physics for several decades. As the name implies, the conducting electrons form a new periodic modulation with a period that is commensurate or incommensurate with the underlying lattice. This phenomenon is usually induced by Fermi surface nesting (FSN), where the Fermi surface tends to nest between nearly parallel parts connected by a vector $\mathbf{q} = 2\mathbf{k}_F$, which causes the electronic susceptibility to diverge at the nesting wave vector [1]. Meanwhile, the lattice responds to the electronic condensate through electron-phonon coupling. At $\mathbf{q} = 2\mathbf{k}_F$, acoustic phonons tend to be softened to zero frequency, which further gives rise to the periodic modulation of the lattice structure [2–5]. In the CDW state, a single-particle energy gap will open in the nested region of the Fermi surface, leading to the lowering of the electronic energy of the system. Therefore the experimental characterization of the single-particle energy gap would be a key step in identifying the CDW state, which can be realized by optical conductivity spectroscopy. Besides single-particle excitation, CDWs also have collective excitations consisting of an amplitude mode and a phase mode. The amplitude mode corresponds to the ionic displacement with a finite gap at the $\mathbf{q} = 0$ limit and behaves like optical phonons [6,7]. In this regard, measurement of the amplitude mode can also be important evidence of CDW phase transition, which has been verified by both pump-probe and Raman spectroscopy [8–11].

Generally, CDWs tend to exist in low-dimensional systems. Typical examples include $K_{0.3}MoO_3$ [12], transition-metal dichalcogenides [10,13], rare-earth tritellurides [14,15], etc. Among all these materials, the underlying CDW mechanism matches very well with the established theory, providing standard systems to study new CDW materials. Recently, the compound CuTe was reported to be a new CDW material, which has attracted attention for it is a rare two-dimensional (2D) layered material hosting quasi-1D CDW order. Its structure is similar to the well-known prototype Fe-based superconductor FeSe. There exists a small difference between in-plane lattice parameters *a* and *b*, resulting in an orthorhombic lattice structure. It exhibits period modulation corresponding to Te chains at low temperature, indicating a CDW phase transition [16]. Angle-resolved photoemission spectroscopy (ARPES) has identified CuTe as a CDW metal with an anisotropic gap below transition temperature 335 K [17]. The nested Fermi surface that drives CDW transition is observed to emerge from nearly parallel line Fermi segments, which is connected by CDW wave vector $\mathbf{q}_x = 0.4a^*$. Based on the Seebeck coefficient, thermal conductivity, and specific heat measurement, Kuo *et al.* reported that CDW order can have a great influence on the thermal transport properties, due to strong electron-phonon coupling [18]. Additionally, by application of external pressure, the CDW transition temperature T_{CDW} of CuTe decreases gradually [19]. With increasing pressure, superconductivity emerges at 2.4 K after the CDW gets suppressed completely, suggesting that the CDW order competes with superconductivity in CuTe [19]. Despite these experimental results, the electrical and optical response of

*nlwang@pku.edu.cn

CuTe along the *b* axis remains unclear. It is highly interesting to investigate how the CDW phase transition affects the anisotropic properties of the 2D layered material, in particular, on the transport and optical conductivity properties.

In this paper, we use a combination of transport, optical spectroscopy, and ultrafast pump-probe reflectivity studies of single-crystalline CuTe. Optical spectroscopy is a valuable experimental method that probes the bulk properties of materials, including the charge dynamics and electronic band structure of a system. On the other hand, ultrafast spectroscopy can probe coherent vibrational dynamics with high resolution to approach a low energy scale. Furthermore, the energy gap arising from CDW order plays an important role in the relaxation process of quasiparticles. The relaxation time and amplitude of quasiparticles show strong enhancement near the transition temperature, which could also be probed from the pump-probe measurements. From optical spectroscopy, we find that there appears an energy gap along the *a* axis which dramatically reduces the carrier density across T_{CDW}, while it behaves as a usual metal along the *b* axis without showing any anomaly below T_{CDW}. The amplitude and the relaxation of photoinduced carriers exhibit a quasidivergence behavior, yielding further evidence for CDW energy gap formation. Moreover, photoinduced reflectivity displays strong oscillation signals on top of the decay process at low temperatures. One of the oscillations has a much higher signal intensity, and its energy softens by over 18% upon heating from 4.6 to 280 K. The temperature dependence of the oscillation suggests that it arises from the amplitude mode of CDW collective excitation.

II. EXPERIMENTAL RESULTS

Single crystals of CuTe were grown by melting stoichiometric amounts of Cu and Te at 500 °C. After 24 h, the melt was cooled to 400 °C at a rate of 4 °C/h. Then the furnace was shut down and cooled to room temperature. The crystal has a flakelike shape with a shining *ab* plane as the cleavage plane, consistent with its quasi-2D structure. We can identify the crystallographic *a* axis perpendicular to the striplike structure, determined using a Laue x-ray diffractometer.

CuTe is composed of a stack of edge-sharing $CuTe_4$ tetrahedra layer by layer with space group *Pmmn* and orthorhombic lattice constants of $a = 3.124$ Å, $b = 4.086$ Å, and $c = 6.946$ Å [20]. Figure 1(a) shows the top view of the crystal of CuTe projected on the *ab* plane, where Cu atoms and Te atoms form a rectangle-shaped lattice. In the normal state, the Te atoms form a quasi-1D chain along the *a* axis where the bond length is shorter than that along the *b* axis, which runs above and below the puckered Cu layers with an equal Te-Te distance as shown in Fig. 1(b). Below the transition temperature, units of two or three Te atoms (marked by red dashed lines) with shorter distances [movement of atoms indicated by black arrows in Fig. 1(b)] alternate with single Te atoms along the *a* axis. Meanwhile, the modulation of the Te position forces corrugated Cu layers to have a slight distortion along the *c* axis, resulting in a $5 \times 1 \times 2$ superstructure [16].

The temperature-dependent resistivity measurement was performed with a standard four-probe method using a Quantum Design physical property measurement system (PPMS). Figure 2(a) displays the resistivity with currents flowing along the crystallographic *a* and *b* axes, respectively. When the electric current flows along the *a* axis, the resistivity shows metallic behavior in the entire measured range except for a sudden upturn that appears at 335 K. This resistivity anomaly is a result of CDW transition, which is consistent with a previous report [17]. In contrast, we did not find a resistivity anomaly along the *b* axis within our measurement resolution. The resistivity data suggest that the CDW order is completely absent in the *b* axis, which is quite rare in a highly 2D system.

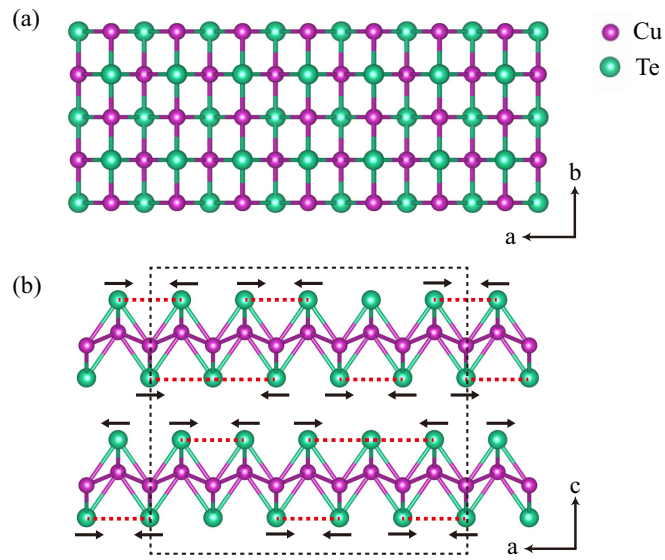

FIG. 1. Crystal structures of CuTe. (a) Top view and (b) side view of the non-CDW phase. Arrows indicate the movement of Te atoms in the CDW phase.

We performed polarized optical reflectance measurements with **E** parallel to the *a* axis and **E** parallel to the *b* axis, respectively, on a Bruker 80-V Fourier transform infrared spectrometer in the frequency range from 30 to 30 000 cm^{-1}. An in-suit gold and aluminum overcoating technique was used to get the reflectivity $R(\omega)$. At 345 K, the reflectivity along the *a* axis and *b* axis over a broad frequency is plotted in Fig. 2(b). Both directions show good metallic behavior in agreement with the dc-resistivity measurement, since reflectivity reaches almost unity at low frequency with a large plasma edge. Note that the reflectivity shows a tremendous difference in edge frequency, suggesting that this compound is highly anisotropic. The edge frequency, referred to usually as the "screened" plasma frequency, is related to the density *n* and effective mass m^* of free carriers by $\omega_p'^2 \propto n/m^*$. The larger plasma frequency along the *a* axis is consistent with a previous report that the conductivity along the chain direction is larger than the conductivity perpendicular to the chain at room temperature [21].

The temperature-dependent reflectivity along the *a* and *b* axes is displayed in Figs. 3(a) and 3(b), respectively. Let us first discuss the optical response along the *a* axis. Firstly, the low-energy reflectivity reaches almost unity. Additionally,

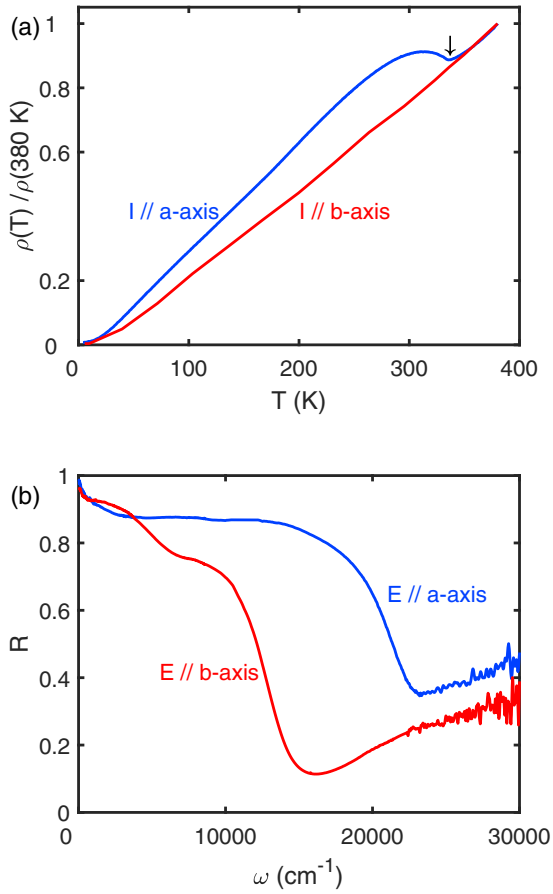

FIG. 2. (a) The temperature-dependent resistivity of CuTe measured with currents flowing along the crystallographic a and b axes, normalized at 380 K. (b) Optical reflectivity $R(\omega)$ in a broad range at 345 K, along the a and b axes, respectively.

when the temperature decreases, the low-energy reflectivity increases. Both features show that the sample has a highly metallic nature, in agreement with the dc-resistivity measurement. When the temperature decreases, the most significant feature in spectra $R(\omega)$ is the substantial suppression in the midinfrared region, which is a typical optical signature of a charge gap formation corresponding to CDW phase transition. The reflectivity exhibits a steep plasma edge around 1800 cm^{-1}, revealing that the density of free carriers is substantially suppressed. In the meantime, the scattering rate is also significantly reduced. The dip becomes more dramatic at low temperatures, suggesting that the energy gap is further enhanced.

The real part of the conductivity was derived from $R(\omega)$ through Kramers-Kronig transformation, as shown in Fig. 3(c). The conductivity consists of a Drude peak at zero frequency and several other Lorentz peaks at a finite frequency in the whole measurement temperature range. At high temperatures, the Drude peak is rather broad demonstrating a large scattering rate of the free carriers. Upon entering the low-temperature phase, the spectral weight of the Drude peak is substantially removed and transfers to higher energies to form a broad peak around 4000 cm^{-1}. The Drude peak narrows continuously with decreasing temperature, implying suppressed quasiparticle scattering. Meanwhile, the positions of the Lorentz peak move to a higher frequency as a result of the further enhancement of the energy gap. In fact, these behaviors are supposed to be the contribution of the case I coherent factor for density wave order [22]. We can roughly estimate the scale of the CDW gap through the edge position of the peak, which locates at 4000 cm^{-1} (500 meV). In an earlier ARPES measurement, an anisotropic energy gap with a maximum value of 190 meV was identified. It should be noted that ARPES measures the gap relative to the Fermi level, while optical spectroscopy measures the interband transition from the occupied state to the unoccupied state above the Fermi level. The gap value determined by optics usually doubles the energy gap obtained by ARPES if the Fermi level is in the center of the gap. Nevertheless, the energy gap determined by optics can only be taken as a rough estimation because it is hard to determine accurately the conductivity edge. Taking the transition temperature $T_c = 335$ K, we can get the ratio $2\Delta/k_B T_c = 17$, which is similar to that reported in other CDW materials, e.g., $TbTe_3$ [15], and is much larger than the weak-coupling theory prediction [2].

To get more information quantitatively, we use the Drude-Lorentz model to decompose the conductivity into different components:

$$\sigma_1(\omega) = \frac{\omega_p^2}{4\pi}\frac{\Gamma_D}{\omega^2+\Gamma_D^2} + \sum_j \frac{S_j^2}{4\pi}\frac{\Gamma_j\omega^2}{\left(\omega_j^2-\omega^2\right)^2+\omega^2\Gamma_j^2}. \quad (1)$$

The first term is the Drude components, attributed to the intraband transition of itinerant carriers, while the second term is the Lorentz components, which correspond to the interband transition and excitation across energy gaps [9]. The inset of Fig. 3(c) presents the fitting results along the a axis at 10 K. The spectrum of 345 K can be well reproduced by one Drude and one Lorentz term. At low temperature, one additional Lorentz term needs to be added to reproduce the peak at 4500 cm^{-1}. As mentioned above, the variation of plasma frequency ω_p is proportional to $\sqrt{n/m^*}$. From our fitting date, the plasma frequency varies roughly from 48 000 cm^{-1} at 345 K to 22 000 cm^{-1} at 10 K. Assuming that the effective mass of free carriers is constant at different temperatures, the reduction of the plasma frequency indicates that 78% free carriers are removed by the opening of the CDW energy gap. Meanwhile, the scattering rate γ, i.e., the width of the Drude peak, decreases dramatically from 2100 to 265 cm^{-1} at low temperature. Consequently, it is reasonable that the compound still behaves like metal even though more than half of the free carriers are lost due to the formation of a CDW energy gap.

In contrast, the reflectivity and the real part of the optical conductivity along the b axis, as shown in Figs. 3(b) and 3(d), do not exhibit these behaviors, but just behave like a simple metal at all temperatures investigated. The scattering rate decreases monotonically upon cooling. There are no signatures of gap formation along the b axis in the optical spectroscopy measurements, consistent with CDW formation along the chain direction.

In order to get further information on the CDW transition, we performed ultrafast pump-probe measurements on this compound, which have been proven to be particularly powerful in detecting both the single-particle excitations across

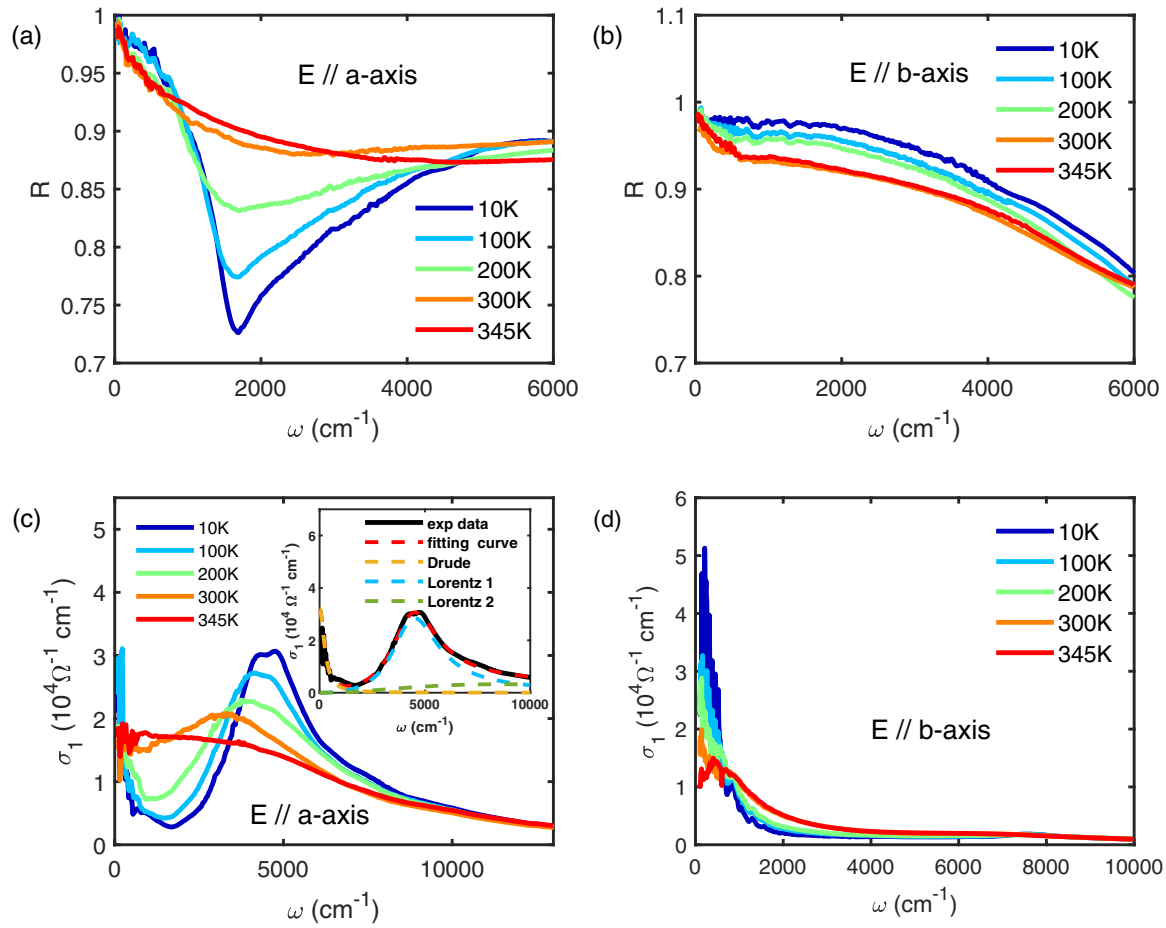

FIG. 3. The temperature-dependent optical reflectivity $R(\omega)$ along the a axis (a) and b axis (b), respectively. The optical conductivity σ_1 at different temperatures along the a axis (c) and b axis (d), respectively. The inset of (c) displays $\sigma_1(\omega)$ along the a axis at 10 K together with a Drude-Lorentz fit.

small energy gaps [23,24] and the collective excitations relevant to long-range ordering [25–27]. We used a Ti:sapphire oscillator as the light source for both pump and probe beams, which can produce 800-nm laser pulses with 100 fs width and 80 MHz repetition rate. The fluence of the pump beam is about 4 μJ/cm^2, while the fluence of the probe beam is ten times lower. The polarization directions of the pump and probe pulse are perpendicular to each other, in order to eliminate the interference. We measured photoinduced transient reflectivity $\Delta R/R$ with the electric field **E** direction of the probe beam parallel to the crystallographic a axis.

The time-dependent $\Delta R/R$ along the a axis at several selected temperatures are displayed in Figs. 4(a) and 4(b). Each spectrum initially increases in a very short time induced by the pump excitation and then drops back to the equilibrium state within picoseconds. The relaxation process can be described by a single exponential decay and a constant $\Delta R/R = A\exp(-t/\tau) + C$, where A represents the amplitude of the photoinduced reflectivity change and τ stands for the relaxation time for photon-excited carriers to decay to their original states. The constant C indicates a long relaxation time arising from thermal diffusion, where energy from the electrons transfers to the environment.

Above the transition temperature, the amplitude A and relaxation time τ depend mildly on temperature, while both of them are strongly enhanced by entering the CDW state. The temperature-dependent A and τ can be extracted by single exponential fitting for various temperatures, which is plotted in Figs. 4(c) and 4(d), respectively. The amplitude and relaxation time display anomalies near the transition temperature. We also tried to fit the $\Delta R/R$ using a convolution between an exponential decay function and a Gaussian response function and found that the fitting results were almost unchanged. The amplitude A drops sharply, while the relaxation time τ shows a continuous divergence at 330 K. This anomaly behavior of the relaxation process can arise from the energy gap opening, as will be explained in detail later.

Here, we employ the Rothwarf-Taylor (RT) model to interpret the decay of the photoexcited quasiparticles (QPs) [28]. The RT model was first proposed to resolve the ultrafast relaxation mechanism in superconductivity. It was proved to be applicable for a wide range of materials with a gap opening in the density of states. Photoexcitation would generate a large number of QPs, which would decay via electron-electron or electron-phonon interactions towards the initial equilibrium state. The formation of an energy gap would introduce a bottleneck effect, which would significantly impede the relaxation of QPs. The bottleneck effect is that when QPs recombine across an energy gap, high-energy phonons are generated, which could also induce a large number QPs in

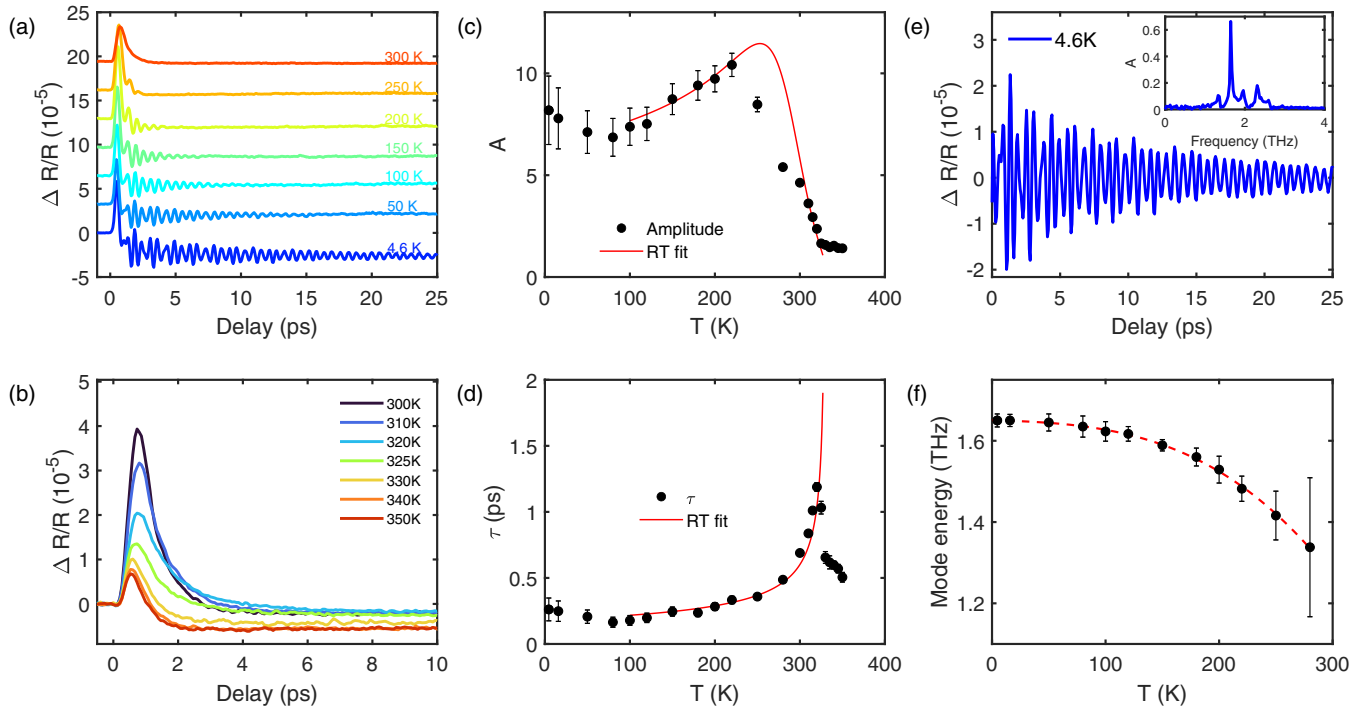

FIG. 4. (a) and (b) The photoinduced reflectivity $\Delta R/R$ along the a axis as a function of time delay at several selected temperatures. Curves in (a) are vertically shifted for clarity. (c) and (d) The amplitude A and relaxation time τ of the fast decay process extracted from the exponential fitting to the experimental data of $\Delta R/R$ at different temperatures. Error bars represent the standard deviation of the fit. The red curves are fitting curves from Eqs. (2) and (3) below the phase transition temperatures. (e) The oscillation part of $\Delta R/R$ at 4.6 K after subtracting the decay background. The inset presents the fast Fourier transformation of the oscillation. (f) The temperature-dependent frequencies of the CDW amplitude mode. The red dashed curve is a guide to the eye.

return, leading to a long relaxation time. Based on this model, the density of thermally activated quasiparticles n_T can be obtained via the amplitude $A(T)$, $n_T \propto [A(T)/A(T \to 0)]^{-1} - 1$. Considering the relationship between n_T and $\Delta(T)$, $n_T \propto \sqrt{\Delta(T)T}\exp[-\Delta(T)/T]$, where $\Delta(T) = \Delta(0)\sqrt{1 - T/T_c}$, we can get [29]

$$A(T) \propto \frac{\Phi/(\Delta(T) + k_B T/2)}{1 + \gamma\sqrt{2k_B T/\Delta(T)}\exp[-\Delta(T)/k_B T]}, \quad (2)$$

where Φ is the pump fluence and γ is a fitting parameter.

As the temperature rises, more and more low-energy phonons become available to break condensed carriers with a reduction of the energy gap, which causes the relaxation time of QPs to diverge at the transition temperature. In the RT model, the relaxation rate near T_c is dominated by the energy transfer from high-frequency phonons with $\omega > 2\Delta$ to low-frequency phonons with $\omega < 2\Delta$. The phonon relaxation rate can be expressed as [29]

$$\frac{1}{\tau} = \frac{12\Gamma_\omega k_B T' \Delta(T)}{\hbar\omega^2}, \quad (3)$$

where Γ_ω is Raman phonon linewidth and T' is the QP temperature. Apparently, $\tau(T) \propto \Delta(T)^{-1}$ in the vicinity of T_c; thus a divergence is expected at the phase transition temperature where the energy gap starts to open. Qualitatively, these equations can reproduce the measurement results around T_c. In the high-temperature limit, we take $\omega = 1.65$ THz as the phonon frequency and $T' = 330$ K as the QP temperature. The best fits yield the phenomenological fitting parameter $\gamma \approx 100$ and $\Gamma_\omega \approx 10$ cm^{-1}, as shown in Figs. 4(c) and 4(d).

On the other hand, the transient reflectivity $\Delta R/R$ exhibits pronounced oscillatory signals at low temperatures arising from the coherent phonon. The lifetime and periods of the coherent phonon change with temperature variation. To analyze the component quantitatively, we first subtract the exponential fitting part and then perform a fast Fourier transformation of the residual oscillation part. As an example, Fig. 4(e) displays $\Delta R/R$ data at 4.6 K as a function of time delay within 25 ps after subtracting the decay background. The inset shows the Fourier transform of the residual part. Five distinct peaks are observed in the Fourier spectrum at 1.32, 1.65, 1.96, 2.31, and 2.59 THz. Based on previous reports, the strength of the CDW amplitude mode is much larger than that of other phonon modes, and its frequency would exhibit softening on approaching T_c. Indeed, here the mode at 1.65 THz has a much larger strength and shows significant softening at elevated temperature as shown in Fig. 4(f). Compared with the 1.65-THz mode, the other four modes decay rapidly with the increase in temperature. We can no longer resolve them above 150 K, while their energy keeps nearly unchanged within our measurement resolution. Therefore we identify the 1.65-THz phonon as a CDW amplitude mode. In principle, the 1.65-THz phonon should be softened to zero at the phase transition temperature. However, since the phonon mode is heavily damped at elevated temperatures as reported before, the CDW amplitude mode only softens to 1.34 THz, and it could not be resolved above 280 K.

III. CONCLUSION

To conclude, by combining transport, optical spectroscopy, and ultrafast pump-probe spectroscopy studies, we provide further evidence of anisotropic quasi-1D CDW phase transition in a CuTe single crystal. A strong anomaly near 335 K in the resistivity is seen only along the *a* axis, while the feature is completely absent along the *b* axis. Our polarized optical measurements show that the optical responses along the *a* and *b* axes are very different, where the plasma frequency with **E** parallel to the *a* axis is much higher than that with **E** parallel to the *b* axis. When **E** is parallel to the *a* axis, the real part of the optical conductivity clearly reveals the formation of an energy gap with associated spectral weight change. In contrast, the optical response behaves like a simple metal at all measured temperatures for **E** parallel to the *b* axis. Furthermore, the amplitude and relaxation time extracted from the photoinduced reflectivity show a sudden enhancement, quite consistent with the RT model prediction, which also confirms the opening of a single-particle energy gap. Meanwhile, we identify the CDW amplitude mode related to the collective excitation of CDW. The spectroscopic information revealed by our anisotropic optical measurements should be very helpful for understanding the electronic properties and related physics. Taking account of the rather high CDW phase transition temperature (above room temperature), CuTe offers an ideal system to study CDW physics as well as its interplay with superconductivity.

ACKNOWLEDGMENTS

This work was supported by the National Key Research and Development Program of China (Grant No. 2017YFA0302904) and National Natural Science Foundation of China (Grant No. 11888101).

[1] R. E. Peierls and R. S. Peierls, *Quantum Theory of Solids* (Oxford University Press, Oxford, 1955).
[2] G. Gruner, *Density Waves in Solids* (CRC, Boca Raton, FL, 2018).
[3] H. Ando, T. Yokoya, K. Ishizaka, S. Tsuda, T. Kiss, S. Shin, T. Eguchi, M. Nohara, and H. Takagi, J. Phys.: Condens. Matter **17**, 4935 (2005).
[4] M. D. Johannes and I. I. Mazin, Phys. Rev. B **77**, 165135 (2008).
[5] J. Laverock, S. B. Dugdale, Z. Major, M. A. Alam, N. Ru, I. R. Fisher, G. Santi, and E. Bruno, Phys. Rev. B **71**, 085114 (2005).
[6] J. F. Scott, Rev. Mod. Phys. **46**, 83 (1974).
[7] X. Du, R. Yuan, L. Duan, C. Wang, Y. Hu, and Y. Li, Phys. Rev. B **90**, 104414 (2014).
[8] R. Y. Chen, S. J. Zhang, M. Y. Zhang, T. Dong, and N. L. Wang, Phys. Rev. Lett. **118**, 107402 (2017).
[9] T. Lin, L. Y. Shi, Z. X. Wang, S. J. Zhang, Q. M. Liu, T. C. Hu, T. Dong, D. Wu, and N. L. Wang, Phys. Rev. B **101**, 205112 (2020).
[10] J. C. Tsang, J. E. Smith, and M. W. Shafer, Phys. Rev. Lett. **37**, 1407 (1976).
[11] Y. Hu, F. Zheng, X. Ren, J. Feng, and Y. Li, Phys. Rev. B **91**, 144502 (2015).
[12] J. P. Pouget, B. Hennion, C. Escribe-Filippini, and M. Sato, Phys. Rev. B **43**, 8421 (1991).
[13] N. V. Smith, S. D. Kevan, and F. J. DiSalvo, J. Phys. C: Solid State Phys. **18**, 3175 (1985).
[14] R. G. Moore, V. Brouet, R. He, D. H. Lu, N. Ru, J.-H. Chu, I. R. Fisher, and Z.-X. Shen, Phys. Rev. B **81**, 073102 (2010).
[15] R. Y. Chen, B. F. Hu, T. Dong, and N. L. Wang, Phys. Rev. B **89**, 075114 (2014).
[16] K. Stolze, A. Isaeva, F. Nitsche, U. Burkhardt, H. Lichte, D. Wolf, and T. Doert, Angew. Chem., Int. Ed. **52**, 862 (2013).
[17] K. Zhang, X. Liu, H. Zhang, K. Deng, M. Yan, W. Yao, M. Zheng, E. F. Schwier, K. Shimada, J. D. Denlinger, Y. Wu, W. Duan, and S. Zhou, Phys. Rev. Lett. **121**, 206402 (2018).
[18] C. N. Kuo, R. Y. Huang, Y. K. Kuo, and C. S. Lue, Phys. Rev. B **102**, 155137 (2020).
[19] S. Wang, X. Chen, C. An, Y. Zhou, Y. Zhou, C. Gu, L. Zhang, X. Yang, and Z. Yang, Phys. Rev. B **103**, 134518 (2021).
[20] S. Seong, T. A. Albright, X. Zhang, and M. Kanatzidis, J. Am. Chem. Soc. **116**, 7287 (1994).
[21] G. Grüner, Rev. Mod. Phys. **60**, 1129 (1988).
[22] M. Dressel and G. Grüner, *Electrodynamics of Solids: Optical Properties of Electrons in Matter* (Cambridge University Press, Cambridge, 2002).
[23] J. Demsar, B. Podobnik, V. V. Kabanov, T. Wolf, and D. Mihailovic, Phys. Rev. Lett. **82**, 4918 (1999).
[24] E. E. M. Chia, D. Talbayev, J.-X. Zhu, J. D. Thompson, A. J. Taylor, H. Q. Yuan, T. Park, C. Panagopoulos, G. F. Chen, J. L. Luo, and N. L. Wang, Phys. Rev. Lett. **104**, 027003 (2010).
[25] R. V. Yusupov, T. Mertelj, J.-H. Chu, I. R. Fisher, and D. Mihailovic, Phys. Rev. Lett. **101**, 246402 (2008).
[26] W. Albrecht, T. Kruse, and H. Kurz, Phys. Rev. Lett. **69**, 1451 (1992).
[27] J. Qi, T. Durakiewicz, S. A. Trugman, J.-X. Zhu, P. S. Riseborough, R. Baumbach, E. D. Bauer, K. Gofryk, J.-Q. Meng, J. J. Joyce, A. J. Taylor, and R. P. Prasankumar, Phys. Rev. Lett. **111**, 057402 (2013).
[28] A. Rothwarf and B. N. Taylor, Phys. Rev. Lett. **19**, 27 (1967).
[29] V. V. Kabanov, J. Demsar, B. Podobnik, and D. Mihailovic, Phys. Rev. B **59**, 1497 (1999).